Effect of surface solidification on the emplacement of lava flows on a slope

A. W. Lyman[1] and R. C. Kerr[1]

Received 30 October 2005; revised 18 January 2006; accepted 28 February 2006; published 31 May 2006.

[1] The emplacement dynamics of lava flows on a slope is investigated using theoretical analyses and laboratory experiments for the case where a fixed volume of lava is rapidly released and propagates downhill as a two-dimensional flow. When the lava has no internal yield strength, we identify four dynamical flow regimes that can arise: an inertial slumping regime, a horizontal viscous regime, a sloping viscous regime, and a crust yield strength regime that finally stops the flow. When the lava has an internal yield strength, it can also flow in a sloping viscoplastic regime which is accurately predicted by a simple box model that we derive. Our results are applied to predict the propagation downhill of various volumes of two typical lavas: a Hawaiian lava with no internal yield strength and a Mount Etna lava with an internal yield strength. In particular, we find that sloping flows of the Mount Etna lava are stopped by the surface crust strength rather than the internal yield strength.

Citation: Lyman, A. W., and R. C. Kerr (2006), Effect of surface solidification on the emplacement of lava flows on a slope, *J. Geophys. Res.*, *111*, B05206, doi:10.1029/2005JB004133.

1. Introduction

[2] Over the past two decades, a number of approaches have been used to model lava or mudflows on either horizontal or sloping surfaces [*Griffiths*, 2000]. Since lava flows are typically much longer than they are thick, most theoretical approaches have used lubrication theory to simplify the governing equations, for flows of viscous fluids [*Huppert*, 1982b; *Lister*, 1992], viscoplastic fluids [*Johnson*, 1970; *Hulme*, 1974; *Lui and Mei*, 1989; *Blake*, 1990; *Huang and Garcia*, 1998; *Balmforth et al.*, 2000; *Osmond and Griffiths*, 2001; *Mei and Yuhi*, 2001; *Balmforth et al.*, 2002] and temperature-dependent viscoplastic fluids [*Balmforth and Craster*, 2000; *Balmforth et al.*, 2004]. In addition, dimensional scaling arguments [*Griffiths and Fink*, 1993] have been used to derive dynamical laws that predict the effect of a surface crust on the rate of propagation of lava flows.

[3] Analogue laboratory experiments have used silicone oils or syrups to study viscous flows [*Huppert*, 1982b; *Lister*, 1992; *Stasiuk et al.*, 1993; *Lister and Kerr*, 1994] and water-kaolin slurries to study viscoplastic flows [*Hulme*, 1974; *Lui and Mei*, 1989; *Blake*, 1990; *Huang and Garcia*, 1998; *Balmforth et al.*, 2000; *Osmond and Griffiths*, 2001]. To model the growth of a surface crust on an actively spreading lava flow, laboratory experiments have used polyethylene glycol wax (PEG) or PEG-kaolin slurries, which cool and solidify as they flow under cold water. These experiments have determined the range of possible flow morphologies that can arise, depending on the flow rate, the cooling rate and the slope [*Hallworth et al.*, 1987; *Fink and Griffiths*, 1990; *Griffiths and Fink*, 1997; *Gregg and Fink*, 2000; *Griffiths et al.*, 2003; *Lyman et al.*, 2004; *Cashman et al.*, 2006]. Surface solidification experiments have also explored transitions between the various dynamical flow regimes. *Blake and Bruno* [2000] have shown that the morphological transition from a uniform lava flow to a compound lava flow corresponds to the dynamical transition from the viscous flow regime to the surface crust controlled flow regime. In a recent study of fixed volume releases in a horizontal channel [*Lyman et al.*, 2005], we found that solidifying flows with no internal yield strength can initially spread in an inertial slumping regime and a viscous flow regime, before a final regime where the yield strength of the growing surface crust stops the flow. We also demonstrated that solidifying flows with an internal yield strength can be stopped by either the internal yield strength or the growing surface crust.

[4] In this paper we extend *Lyman et al.* [2005] by considering surface solidification on the flow of a fixed volume of fluid released in a sloping channel. In section 2, we present the isothermal flow regimes. We first summarize the inertial and viscous flow regimes on a horizontal surface, before introducing the sloping viscous flow regime. We then develop a box model that describes the viscoplastic flow on a slope of a fluid with an internal yield strength. In section 3, the impact of surface cooling and solidification is considered. We predict that the surface crust continues to grow until its strength is great enough to abruptly stop the flow. In section 4, we introduce laboratory experiments that we performed to test our theoretical models. Our experimental results for an isothermal viscoplastic fluid are given in section 5, followed by our results for solidifying viscous

[1]Research School of Earth Sciences, Australian National University, Canberra, ACT, Australia.

0148-0227/06/2005JB004133$09.00

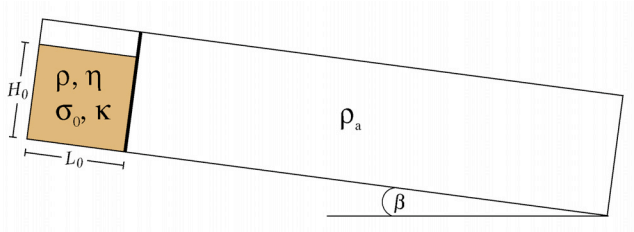

Figure 1. Schematic drawing of the experimental apparatus used to instantaneously release of a fixed volume of fluid per unit width $q = L_0 H_0$ onto a slope β. The released fluid has a density ρ, a viscosity η, a yield strength σ_0 and a thermal diffusivity κ, while the ambient fluid has a density ρ_a.

fluids (in section 6) and our results for solidifying viscoplastic fluids (in section 7). In section 8, we demonstrate how the various flow regimes and theoretical models can be used to predict the emplacement of lava flows. Our conclusions are summarized in section 9.

2. Isothermal Flow Regimes

[5] In this section, we summarize the isothermal flow regimes that can arise during the two-dimensional flow of lava on a slope (or in a sloping channel if sidewall effects are neglected [*Nye*, 1965; *Johnson*, 1970; *Tallarico and Dragoni*, 1999, 2000]). These regimes describe inertial flow, viscous flow, and viscoplastic flow.

[6] As illustrated in Figure 1, we consider the instantaneous release on a slope β of a fixed volume q per unit width. The lava has a density ρ, viscosity η and yield strength σ_0, while the ambient fluid (water or air) has a density ρ_a. The released lava has an initial downslope length L_0 and average height H_0. For simplicity, we assume that the slope is small enough that $\cos\beta \approx 1$ and hence $H_0 = q/L_0$. We also assume that $H_0 \gg L_0 \sin\beta$, so the lava depth is approximately constant in the initial reservoir.

2.1. Inertial Slumping and Viscous Flow

[7] At early times (and for large enough volumes of lava [*Lyman et al.*, 2005]), the initial flow regime is an inertial slumping of the lava under gravity. In this regime, the gravity current moves at a constant velocity, and the flow length L and average height H as a function of time t are given by

$$L = L_0 + c_{sl}\left[\frac{g\Delta\rho}{\rho}H_0\right]^{\frac{1}{2}}t \tag{1}$$

$$H = \frac{q}{L}, \tag{2}$$

where $\Delta\rho = \rho - \rho_a$ and the constant c_{sl} has an experimentally measured value of 0.46 [*Simpson*, 1997]. After the flow has travelled about ten times its initial length, the initial slumping regime may be followed by a self-similar inertial flow regime in which the length $L = 1.6\,(g\Delta\rho q/\rho)^{\frac{1}{5}}t^{\frac{2}{5}}$ [*Rottman and Simpson*, 1983; *Simpson*, 1997]. However, this regime will not develop if viscous stresses become dominant before the gravity current can reach this length. The initial slumping regime can then be followed by two viscous flow regimes, where viscous stresses on the base control the rate of spreading. The first viscous flow regime describes gravity current spreading on a horizontal surface:

$$L = c_v\left[\frac{g\Delta\rho q^3 t}{\eta}\right]^{\frac{1}{5}} \tag{3}$$

$$H = \frac{q}{L} = \frac{1}{c_v}\left[\frac{\eta q^2}{g\Delta\rho t}\right]^{\frac{1}{5}}, \tag{4}$$

where $c_v = 1.13$ [*Pattle*, 1959; *Huppert*, 1982b]. Eventually, however, the viscous gravity current is affected by the slope β, and its spreading is then given by:

$$L = c_{vs}\left[\frac{g\Delta\rho\sin\beta\, q^2 t}{\eta}\right]^{\frac{1}{3}} \tag{5}$$

$$H = \frac{q}{L} = \frac{1}{c_{vs}}\left[\frac{\eta q}{g\Delta\rho\sin\beta\, t}\right]^{\frac{1}{3}}, \tag{6}$$

where $c_{vs} = (3/2)^{2/3} = 1.31$ [*Huppert*, 1982a; *Lister*, 1992].

[8] By equating (3) and (5), the transition from the horizontal viscous flow regime to the sloping viscous flow regime is found to occur at a time

$$t^v_{vs} = \left[\frac{c_v}{c_{vs}}\right]^{\frac{15}{2}}\frac{\eta}{g\Delta\rho\, q^{\frac{1}{2}}\sin^{\frac{5}{2}}\beta} \tag{7}$$

and at a downslope distance

$$L^v_{vs} = \left[\frac{c_v^5 q}{c_{vs}^3\sin\beta}\right]^{\frac{1}{2}} = 0.905\left[\frac{q}{\sin\beta}\right]^{\frac{1}{2}}. \tag{8}$$

Similarly, we can determine the transition from the inertial slumping regime to the horizontal viscous flow regime by equating (1) and (3), and the transition from the inertial slumping regime to the sloping viscous flow regime by equating (1) and (5).

2.2. Viscoplastic Flow on a Slope

[9] In the absence of an internal yield strength (i.e., $\sigma_0 = 0$), the viscous flow will continue without limit, or until topography interferes with its progress. However, if the lava has an internal yield strength, the flow will eventually cease when the gravity current thickness has decreased to [*Hulme*, 1974]

$$H_y = \frac{\sigma_0}{g\Delta\rho\sin\beta}, \tag{9}$$

which implies a final flow length

$$L_y = \frac{q}{H_y} = \frac{qg\Delta\rho\sin\beta}{\sigma_0}. \tag{10}$$

[10] To describe the viscoplastic flow of the gravity current to the final yield strength regime, we propose a simple "box model," in which the current is taken to have a length $L(t)$ and a uniform thickness $H(t) = q/L(t)$ (see *Huppert* [1998] for examples of similar box models used to model the propagation of particle-driven gravity currents). The increasing box length and decreasing box thickness are therefore linked by

$$\frac{\mathrm{d}L}{\mathrm{d}t} = -\frac{q}{H^2}\frac{\mathrm{d}H}{\mathrm{d}t}. \tag{11}$$

The flowing current consists of a lower region of viscous shear flow overlain by an upper region of uniform plug flow with a velocity [e.g., *Lui and Mei*, 1989]

$$U_p = \frac{g\Delta\rho\sin\beta}{2\eta}\left(H - H_y\right)^2. \tag{12}$$

If this plug velocity is used to predict the advance of the box (i.e., $\mathrm{d}L/\mathrm{d}t = U_p$), (11) and (12) can be combined to obtain

$$-\frac{q}{H^2}\frac{\mathrm{d}H}{\mathrm{d}t} = \frac{g\Delta\rho\sin\beta}{2\eta}\left(H - H_y\right)^2. \tag{13}$$

To focus on the slow evolution to the yield strength regime, we define $\xi = (H - H_y)/H_y$ and substitute in (13), giving

$$\frac{\mathrm{d}\xi}{\mathrm{d}t} = -\frac{g\Delta\rho H_y^3\sin\beta}{2q\eta}\xi^2(1+\xi)^2. \tag{14}$$

When we define the timescale

$$\tau = \frac{2q\eta}{g\Delta\rho H_y^3\sin\beta}, \tag{15}$$

(14) then becomes

$$\frac{\mathrm{d}\xi}{\mathrm{d}t} = -\frac{\xi^2(1+\xi)^2}{\tau}. \tag{16}$$

[11] In the final slow approach to the yield strength regime, $\xi \ll 1$ and (16) becomes simply

$$\frac{\mathrm{d}\xi}{\mathrm{d}t} = -\frac{\xi^2}{\tau}, \tag{17}$$

whose solution is

$$\frac{1}{\xi} = \frac{1}{\xi_0} + \frac{t}{\tau}, \tag{18}$$

where $\xi_0 = (H_0 - H_y)/H_y$. The asymptotic solution (18) can alternatively be written

$$\frac{H}{H_y} = \frac{L_y}{L} = 1 + \left(\frac{H_y}{H_0 - H_y} + \frac{t}{\tau}\right)^{-1}. \tag{19}$$

Equations (18) and (19) show that the gravity current approaches the final yield strength regime as a slow algebraic decay that continues for an infinite time, with a timescale given by τ.

[12] The viscoplastic flow at earlier times (and greater flow thicknesses) can also be determined, by integrating (16) to obtain

$$\frac{t}{\tau} = \frac{1}{\xi} - \frac{1}{\xi_0} + \frac{1}{1+\xi} - \frac{1}{1+\xi_0} + 2\ln\left(\frac{\xi(1+\xi_0)}{\xi_0(1+\xi)}\right), \tag{20}$$

which can alternatively be written in terms of $H(t)$ as

$$\frac{t}{\tau} = \frac{H_y}{H - H_y} - \frac{H_y}{H_0 - H_y} + \frac{H_y}{H} - \frac{H_y}{H_0} + 2\ln\left(1 - \frac{H_y}{H}\right) - 2\ln\left(1 - \frac{H_y}{H_0}\right). \tag{21}$$

When $H_0 \gg H_y$, (21) becomes

$$\frac{t}{\tau} = \frac{H_y}{H - H_y} + \frac{H_y}{H} + 2\ln\left(1 - \frac{H_y}{H}\right). \tag{22}$$

3. Flows With Surface Cooling and Solidification

[13] In this section, we examine the effect of cooling and solidification on the emplacement of lava flows on a slope. We assume that the Péclet number is large ($Pe = UH_0/\kappa \gg 1$, where U is the surface flow velocity and κ is the thermal diffusivity of the fluid) so that the cooling and solidification are confined to a thin surface boundary layer. Following *Griffiths and Fink* [1993], we assume that the surface crust thickness δ at the flow front grows diffusively as $\delta \sim (\kappa t)^{\frac{1}{2}}$. If the effective yield strength of the crust is σ_c, then the flow front is able to exert a retarding force per unit width $\sim\delta\sigma_c$. This retarding force can then be equated to the driving buoyancy force per unit width $\sim g\Delta\rho H^2$, to show that the growing surface crust can hold back a flow of height:

$$H = \frac{1}{c_c}\left[\frac{\sigma_c}{g\Delta\rho}\right]^{\frac{1}{2}}(\kappa t)^{\frac{1}{4}}, \tag{23}$$

or in terms of length:

$$L = c_c\left[\frac{g\Delta\rho}{\sigma_c}\right]^{\frac{1}{2}} q\,(\kappa t)^{-\frac{1}{4}} \tag{24}$$

where c_c is an unknown numerical constant of order 1 [*Griffiths and Fink*, 1993].

[14] In sections 3.2 and 3.3 of *Lyman et al.* [2005], we quantified the final runout time and final runout length when it is in either the horizontal slumping regime or the horizontal viscous regime. In the latter case, the the runout time

$$t_c^v = \left(\frac{c_c}{c_v}\right)^{\frac{20}{9}} \frac{(g\Delta\rho)^{\frac{2}{9}} q^{\frac{8}{9}}\eta^{\frac{4}{9}}}{\sigma_c^{\frac{10}{9}}\kappa^{\frac{5}{9}}} \tag{25}$$

Table 1. Parameters for the Sloping Isothermal Viscoplastic Experiments

Experiment	Kaolin, wt %	Slope, deg	H_0, m	L_0, m	H^*, m	L^*, m
SIB-14	40.0	19.5	0.0725	0.0970	0.0055	1.2840
SIB-27	40.0	3.0	0.1520	0.2960	0.0350	1.3350
SIB-29	33.3	3.0	0.1000	0.0800	0.0045	1.8000
SIB-30	38.1	10.0	0.1025	0.1000	0.0060	1.8460
SIB-31	33.3	3.0	0.1345	0.0800	0.0050	2.1530
SIB-32	33.3	3.0	0.1150	0.0800	0.0050	1.9000
SIB-33	38.1	5.0	0.1500	0.1000	0.0120	1.2500
SIB-34	36.4	4.0	0.1285	0.1000	0.0090	1.3800
SIB-35	36.4	5.0	0.1500	0.1000	0.0080	2.0200
SIB-36	34.8	3.0	0.0825	0.1000	0.0070	1.1650
SIB-37	34.8	5.0	0.1000	0.1000	0.0045	2.2000

and the runout length:

$$L_c^v = c_c^{\frac{4}{9}} c_v^{\frac{5}{9}} \frac{(g\Delta\rho)^{\frac{1}{3}} q^{\frac{7}{9}}}{\sigma_c^{\frac{2}{9}} (\kappa\eta)^{\frac{1}{9}}}. \quad (26)$$

We now examine the runout on a slope of a viscous fluid or a fluid with a yield strength.

3.1. Viscous Slope Flow With Solidification

[15] In the sloping viscous flow regime, the runout time and length occur when the decreasing flow depth becomes equal to the growing height that the surface crust can hold back. By equating (6) and (23), we find that the transition time t_c^{vs} from the sloping viscous regime to the crust strength regime is

$$t_c^{vs} = \left(\frac{c_c}{c_{vs}}\right)^{\frac{12}{7}} \left(\frac{\eta q}{\sin\beta}\right)^{\frac{4}{7}} \frac{(g\Delta\rho)^{\frac{2}{7}}}{\sigma_c^{\frac{6}{7}} \kappa^{\frac{3}{7}}}. \quad (27)$$

Substitution of t_c^{vs} into (5) then gives the transition distance

$$L_c^{vs} = c_c^{\frac{4}{7}} c_{vs}^{\frac{3}{7}} \frac{(g\Delta\rho)^{\frac{3}{7}} q^{\frac{6}{7}} \sin^{\frac{1}{7}}\beta}{\sigma_c^{\frac{2}{7}} (\kappa\eta)^{\frac{1}{7}}}. \quad (28)$$

3.2. Viscoplastic Slope Flow With Solidification

[16] In the case of the flow on a slope of a viscoplastic fluid, the thickness $H(t)$ of the flow in our box model is given by (21). Eventually, runout occurs when the decreasing flow thickness becomes equal to the increasing height that the surface crust can hold back (see (23)). By equating (21) and (23), we can solve numerically for the transition time t_c^{vps} and the transition length L_c^{vps}.

4. Laboratory Experiments

[17] The experiments were carried out in two different sloping tanks: a glass tank that was 15 cm wide, 30 cm deep, and 1.8 m long and a Perspex tank that was 25 cm wide, 30 cm deep, and 2.5 m long. The fluids used were polyethylene glycol wax (PEG 600) and various slurries of polyethylene glycol wax mixed with kaolin. These fluids are inexpensive and nonhazardous and have a convenient solidification temperature of about 19°C. They also form an amorphous solid in a manner analogous to the quenching of lava to a glass. The density, viscosity, yield strength and thermal diffusivity of these fluids are listed by *Lyman et al.* [2005] (where we note the correction that "strain" should read "strain rate" in Lyman et al.'s Figure 3).

[18] The experimental procedure was as follows. A removable barrier was placed at various distances from one end of the tank to form a reservoir of length L_0. Polyethylene glycol (PEG) or PEG-kaolin slurry was then poured into the reservoir to the desired depth H_0 (Figure 1). The rest of the tank was left empty (in the isothermal experiments) or was filled with cold fresh or salt water (in the solidification experiments). The depth of the water was set to equalize the pressures at the base on both sides of the barrier. The barrier was then removed by pulling it vertically upward, at a rate slow enough to avoid significant mixing (the removal took about 1–2 s for flows under water and 0.1–0.2 s for flows under air). The motion of the fluids was then recorded using a digital video camera, which enabled us to measure accurately the flow length L as a function of time t. The initial slumping velocity of the flow (from equation (1)) was used to calculate a Reynolds number ($Re = 0.46\,(\rho g \Delta\rho)^{\frac{1}{2}} H_0^{\frac{3}{2}}/2\eta$) for each flow. At the end of each experiment, the final runout length L^* and the flow thickness as a function of distance were measured. In the solidification experiments, the runout time t^* was also clear, because the flow stopped at a well defined time.

5. Results for Isothermal Flows With Yield Strength

[19] These experiments used PEG-kaolin slurries flowing under air. The parameters varied were the proportion of kaolin to PEG, the reservoir dimensions L_0 and H_0 (Table 1), and the underlying slope. At the beginning of each experiment the gate was pulled and the slurry was allowed to slump down the length of the tank (Figure 2). Initially the flows were rapid, with Reynolds numbers of 10–50, and they attained most of their length in the first few seconds of the experiment. However, each experiment was allowed to creep until no motion was noticeable (after ~1 hour).

[20] Near the reservoir, the flows were slightly thicker against the walls, because the slurry was slowed down by friction against the sidewalls as it drained down the channel. The center portion of the flow was not affected by the sidewalls and thus flowed more rapidly and was subsequently thinner. Near the flow front the opposite was true: the flow had a convex upward shape at the center of the channel, where the flow was thickest, and the edges near the walls were thinner. The less viscous slurries (lower wt % kaolin) produced thinner flows that were longer with more rounded flow fronts when viewed from above, while higher viscosity slurries (higher wt % kaolin) produced thicker, shorter flows with more squarish flow fronts.

[21] Figure 3 plots the flow length as a function of time in a typical experiment, together with curves showing the various isothermal flow regimes presented in section 2. A comparison of the theoretical curves indicates that this experimental flow was expected to travel first in the inertial slumping regime (equation (1)), and then in the viscoplastic box model regime (equation (21)), before finally stopping at the yield strength limit (equation (10)).

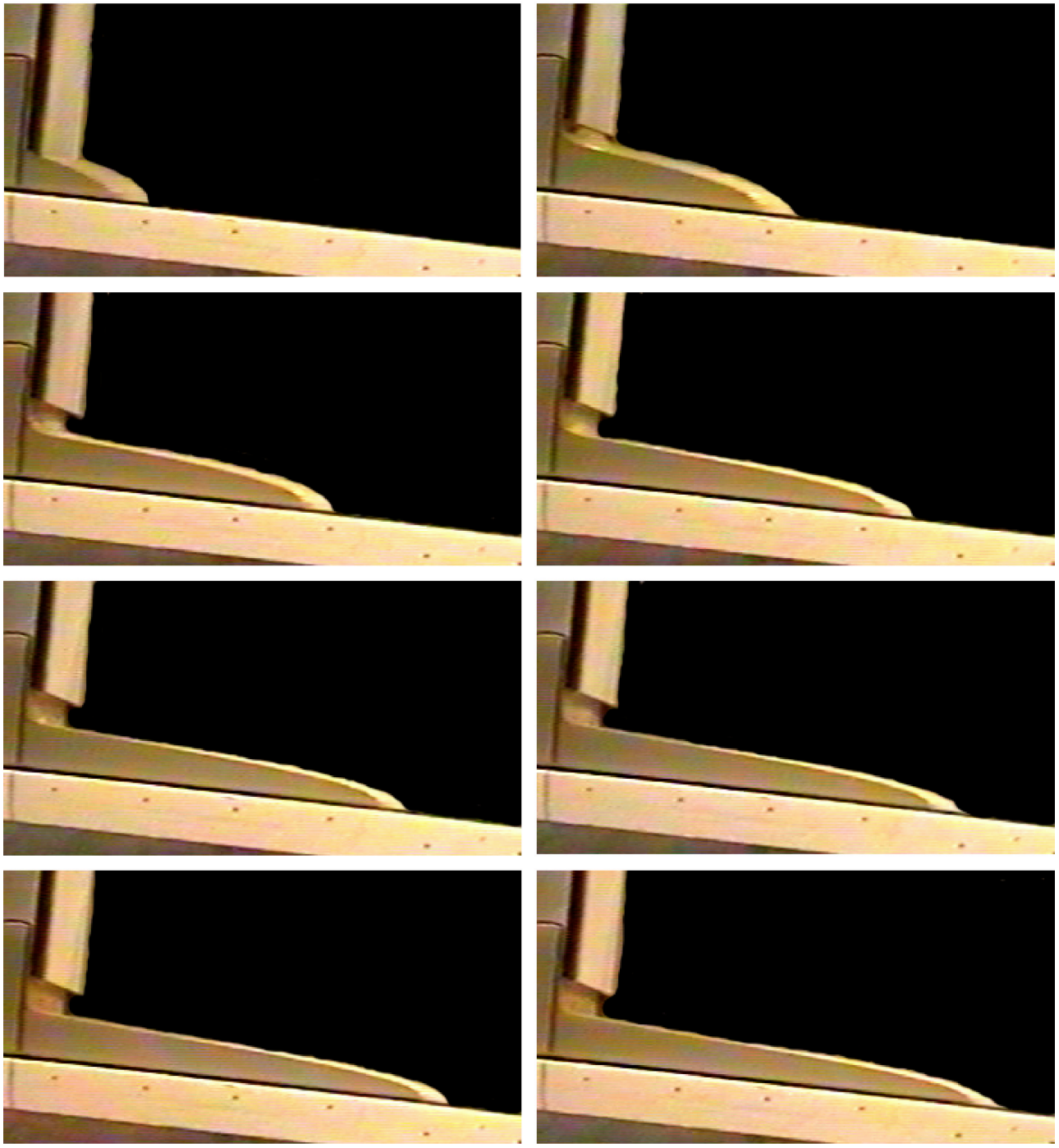

Figure 2. Photographs of a sloping isothermal viscoplastic experiment. The field of view in each frame is about 65 cm. Frames were taken at 0.2, 0.9, 1.6, 2.5, 3.4, 4.2, 5.9, and 7.6 s after the lock was released.

The experimental observations are in excellent agreement with these predictions.

[22] Measurements of the final flow heights H^* and runout lengths L^* at the end of the experiments are given in Figures 4a and 4b, where they are respectively compared with the predicted values of H_y and L_y (compare equations (9) and (10)). The measurements are found to be consistent with the predicted values to within about 10%, which is

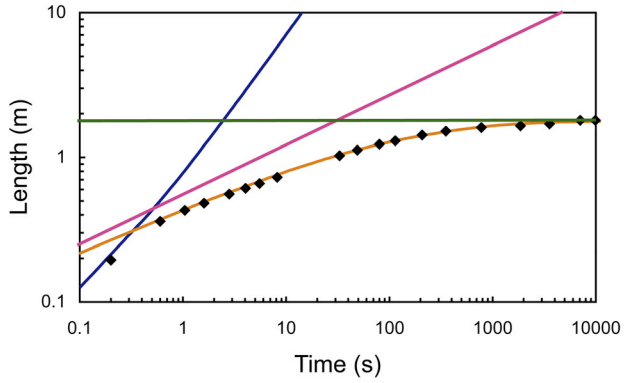

Figure 3. Flow length as a function of time for isothermal yield strength experiment: SIB-29 (33.3 wt % kaolin). The curves show the inertial slumping regime (dark blue line), the sloping viscous flow regime (pink line), the box model of section 2.2 for sloping viscoplastic flow (orange line), and the final yield strength limit (green line). The horizontal viscous flow regime (not shown) plays no role in this experiment, as the transition from horizontal viscous flow to the sloping viscous flow occurs at about 0.1 s, but the flow at that time is still in the inertial slumping regime.

consistent with the estimated 10% uncertainty in the yield strengths used to calculate H_y and L_y.

6. Results for Solidifying Flows Without a Yield Strength

[23] These experiments used PEG flowing under cold salty water. The parameters varied were the slope β, the density difference $\Delta\rho$, the water temperature T_a, the PEG temperature T_l, and the starting depth H_0 (Table 2). In the experiments, significant mixing of the fluids was avoided by ensuring that Ψ_{sl} was less than about 0.5, where

$$\Psi_{sl} = \left[\frac{g\Delta\rho}{\rho H_0}\right]^{\frac{1}{2}} t_s \tag{29}$$

and t_s is the solidification timescale [*Lyman et al.*, 2005]. Some other experiments not listed in Table 2 were also done with different slopes, but they did not show any spreading in the sloping viscous flow regime: when the slope was too large, the flows never got out of the slumping regime before they stopped; and when the slope was too small, the flows remained in horizontal spreading regimes and were unaffected by the slope.

[24] The typical flow behavior is shown in Figure 5. Once the gate was pulled, the PEG advanced rapidly, with Reynolds numbers of 75–200. The front of the flow rapidly froze and was pushed forward by the rest of the flow. As the front reduced in thickness, the flow gradually slowed down, until it finally stopped.

[25] In Figure 6, we show measurements of flow length as a function of time for experiment SCW-12. Initially, the flow followed the slumping regime. After it traveled about 1 m, it then made a transition to the sloping viscous regime, which it then followed until it was abruptly stopped at 1.405 m by the growing surface crust.

[26] The final flow height as a function of distance for three experiments is shown in Figure 7a. The height is found to increase gradually with distance, before dropping rapidly near the flow front. For comparison with Figure 7a, Figure 7b shows the final profiles of three experiments with solidifying PEG on a horizontal base (detailed by *Lyman et al.* [2005]). Here, the height is found to decrease gradually with distance, before dropping rapidly near the flow front.

[27] By setting the unknown numerical constant $c_c = 1$, we can use equation (24) together with the stopping distance L^* and the stopping time t^* to make an order of magnitude estimate of the surface crust strength σ_c:

$$\sigma_c = \frac{g\Delta\rho\, q^2}{(L^*)^2(\kappa t^*)^{1/2}}. \tag{30}$$

The resulting values are listed in Table 2 and plotted as a function of Ψ_{sl} in Figure 8. We find that the surface crust strength has a consistent value of 166 ± 15 Pa, which is in good agreement with the crust strength (160 ± 40 Pa)

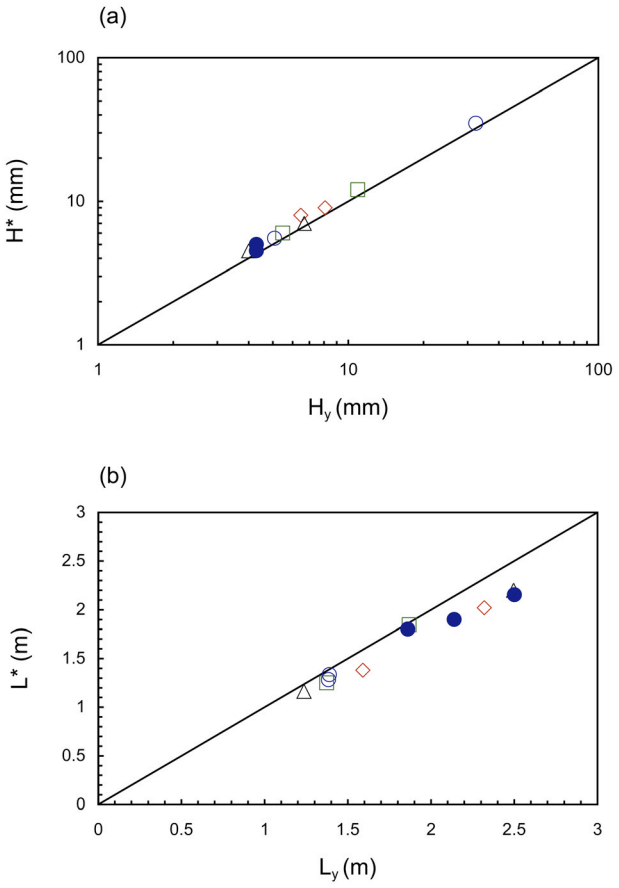

Figure 4. Measurements of the final dimensions of sloping isothermal yield strength flows: (a) the final flow height H^* versus predicted height H_y and (b) the final flow length L^* versus predicted length L_y (solid blue circle 33.3 wt %, black triangle 34.8 wt %, red diamond 36.4 wt %, green square 38.1 wt %, and blue circle 40.0 wt % kaolin). The straight line in each plot represents where the measured final value equals the predicted value.

Table 2. Parameters for the Solidifying PEG Experiments

Experiment	Slope, deg	T_l, °C	T_a, °C	Δρ	H_0, m	L_0, m	L^*, m	t^*, s	Ψ_{sl}	σ_c, Pa
SCW-07	3	25.8	−2.0	13	0.263	0.100	0.760	11.0	0.41	153
SCW-08	3	25.8	−2.3	17	0.263	0.100	0.843	12.0	0.46	156
SCW-09	2	25.0	−5.7	22	0.203	0.100	0.710	12.0	0.34	169
SCW-12	1.5	25.6	−4.2	40	0.300	0.105	1.405	12.5	0.54	186

estimated by *Lyman et al.* [2005] for solidifying PEG experiments on a horizontal base.

7. Results for Solidifying Flows With a Yield Strength

[28] These experiments used PEG-kaolin slurries flowing under cold salty water. The parameters varied were the starting depth H_0, the density difference Δρ, the water temperature T_a, and the slurry temperature T_l (Table 3). In all the experiments, $\Psi_{sl} < 5$, which prevented significant mixing of the fluids [cf. *Lyman et al.*, 2005]. Some other experiments not listed in Table 3 were also done with different slopes and slurry compositions, but they did not show any sloping viscoplastic behavior: when the slope was too large or the slurry too weak, the flows never got out of

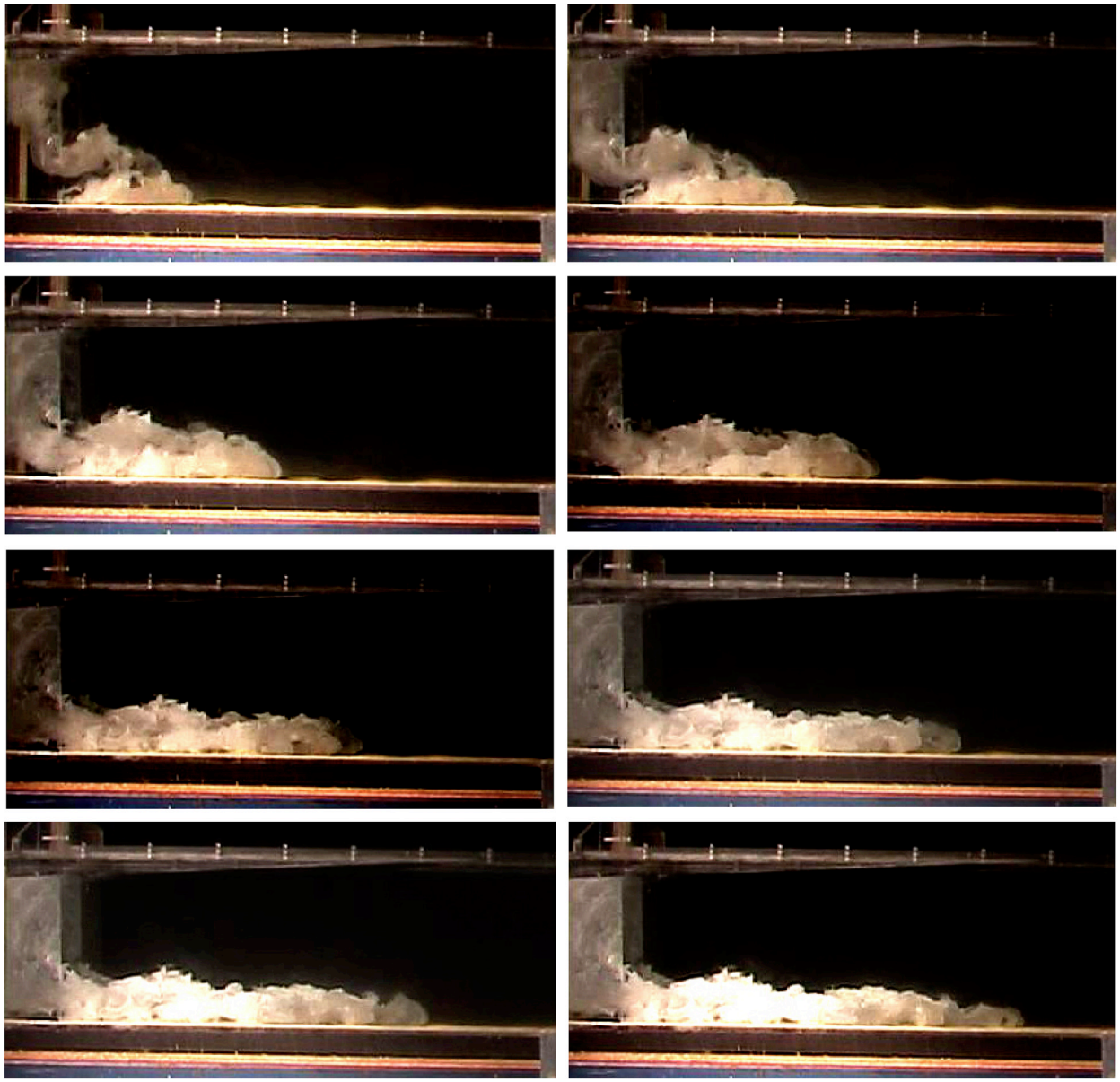

Figure 5. Photographs of the sloping cooling PEG experiment SCW-08. The field of view in each frame is about 1 m. Frames were taken at 2.5, 3.4, 4.6, 5.4, 6.4, 7.4, 8.5, and 9.4 s after the lock was released.

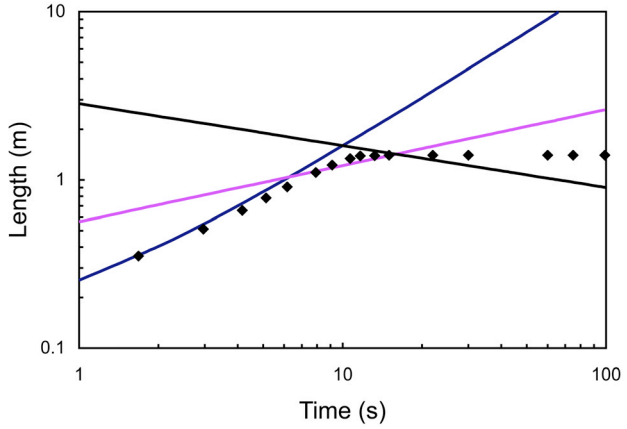

Figure 6. Flow length as a function of time for a solidifying PEG experiment SCW-12 on a slope of 1.5° with $\Psi_{sl} = 0.54$. The curves show the slumping regime (dark blue line), the sloping viscous flow regime (pink line), and the crust strength regime (black line) given by equation (24), where $c_c = 1$ and $\sigma_c = 166$ Pa.

the slumping regime before they stopped; and when the slope was too small or the slurry too strong, the flows remained in horizontal spreading regimes and were unaffected by the slope.

[29] The flows initially looked similar to those in the isothermal viscoplastic experiments in section 5. They advanced rapidly at first (Figure 9), with Reynolds numbers of 25–50. Each experiment formed a rigid crust over its surface, which insulated the rest of the fluid and held any unsolidified slurry in place behind the flow front. If a hole was poked in the crust near the front of the flow, unsolidified slurry began to extrude from it, which showed that the surface crust was responsible for stopping the flow. In some larger volume experiments, rifting of the surface crust was observed (Figure 10). This interesting behavior led to the extrusion of fresh slurry from beneath the solidified crust, creating a smooth surface texture with grooves oriented parallel to the flow direction.

[30] Figure 11 shows the flow length as a function of time for a cooling viscoplastic experiment. Initially, the flow spread in the slumping regime. After about 2 s, the flow made a transition to the sloping viscoplastic regime, which it then followed for about 30 s until it was abruptly stopped at 1.391 m by the growing surface crust, long before it could reach the isothermal yield strength limit of $L_y = 2.028$ m.

[31] Measurements of the final flow height as a function of distance are presented in Figure 12. Figure 12a shows three similar experiments, which had $H_0 \approx 0.154$ m. All three final profiles are very similar. The flow height is nearly constant for the first 0.6 m, but it then starts to increase gradually (up to 51 ± 5 mm) before dropping rapidly near the flow front. Figure 12b shows two larger volume experiments which had $H_0 \approx 0.23$ m. The profiles are very similar, despite the crust rifting and extrusion at about 0.4–0.7 m in experiment SCP-18 (seen in Figure 10). Again, the flow height is nearly constant for the first 0.6 m, but it then starts to increase gradually (up to 58 ± 3 mm) before dropping rapidly near the flow front. For comparison

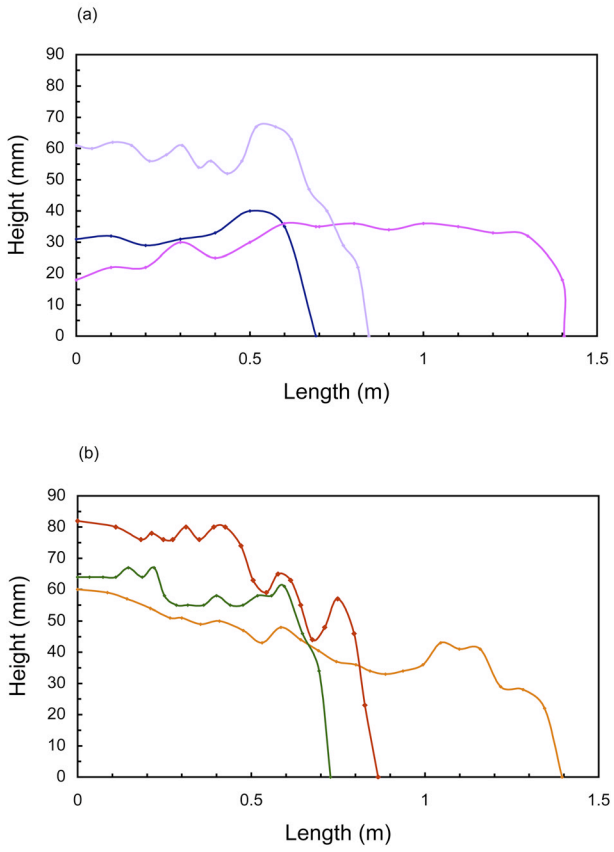

Figure 7. Flow height as a function of length for solidifying PEG experiments. (a) On a slope, SCW-09 (dark blue line), SCW-12 (pink line) and SCW-08 (purple line). (b) On a horizontal base [*Lyman et al.*, 2005], HCN-12 (orange line), HCN-34 (green line), and HCN-11 (red line).

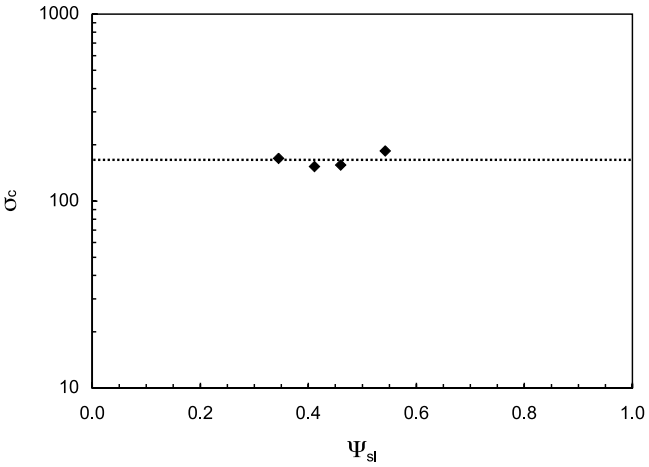

Figure 8. Estimated crust strength σ_c versus Ψ_{sl}, for the solidifying PEG experiments. The strength is constant and has a value of 166 ± 15 Pa, which is represented by the horizontal dotted line.

Table 3. Parameters for the Solidifying Viscoplastic Experiments[a]

Experiment	$\Delta\rho$, kg m^{-3}	T_l, °C	T_a, °C	H_0, m	L_0, m	L_v, m	L^*, m	t^*, s	Ψ_{sl}	σ_c, Pa
SCP-07	269	25.1	−5.5	0.203	0.300	2.759	1.820	41	1.42	1265
SCP-08	271	24.5	−6.5	0.144	0.300	1.970	1.200	46	1.27	1390
SCP-12	263	27.5	−7.8	0.152	0.300	2.018	1.445	46	2.48	1037
SCP-13	260	25.8	−6.3	0.154	0.300	2.028	1.391	55	1.81	1045
SCP-14	259	25.6	−8.5	0.153	0.300	2.007	1.255	45	1.43	1396
SCP-16	264	24.8	−4.9	0.152	0.300	2.026	1.270	45	1.54	1362
SCP-17	260	25.8	−6.3	0.156	0.300	2.048	1.285	46	1.80	1365
SCP-18	262	25.0	−8.4	0.230	0.300	3.052	1.805	77	0.99	1179
SCP-19	261	25.7	−7.7	0.231	0.300	3.047	1.785	87	1.29	1135

[a]These experiments all had a slope of 3° and used 33.3 wt % kaolin.

with Figure 12, Figure 13 shows the final profiles of three experiments with solidifying slurries on a horizontal base (detailed by *Lyman et al.* [2005]). These horizontal flows have very different profiles: they are thickest at the start of the flow and thin greatly toward the flow fronts. The difference between the profiles of sloping and horizontal flows demonstrates that the slope plays an important role in these sloping slurry flows, by allowing the unsolidified slurry to flow downstream toward the front of the flow. The flow therefore spreads further on a slope before the crust is strong enough to stop it.

[32] Using equation (30) together with the measured values of L^* and t^*, we can make an order of magnitude estimate of the surface crust strength σ_c on our solidifying viscoplastic slope flows. The resulting values are listed in Table 3 and plotted as a function of Ψ_{sl} in Figure 14. Previously, we found that the crust strength for solidifying slurry experiments on a horizontal base varied with slurry composition, but not with Ψ_{sl} provided that $\Psi_{sl} < 5$ [*Lyman et al.*, 2005]. In the current sloping experiments, we again find that the crust strength is constant, but the value of 1240 ± 150 Pa is much smaller than the value of 6900 ±

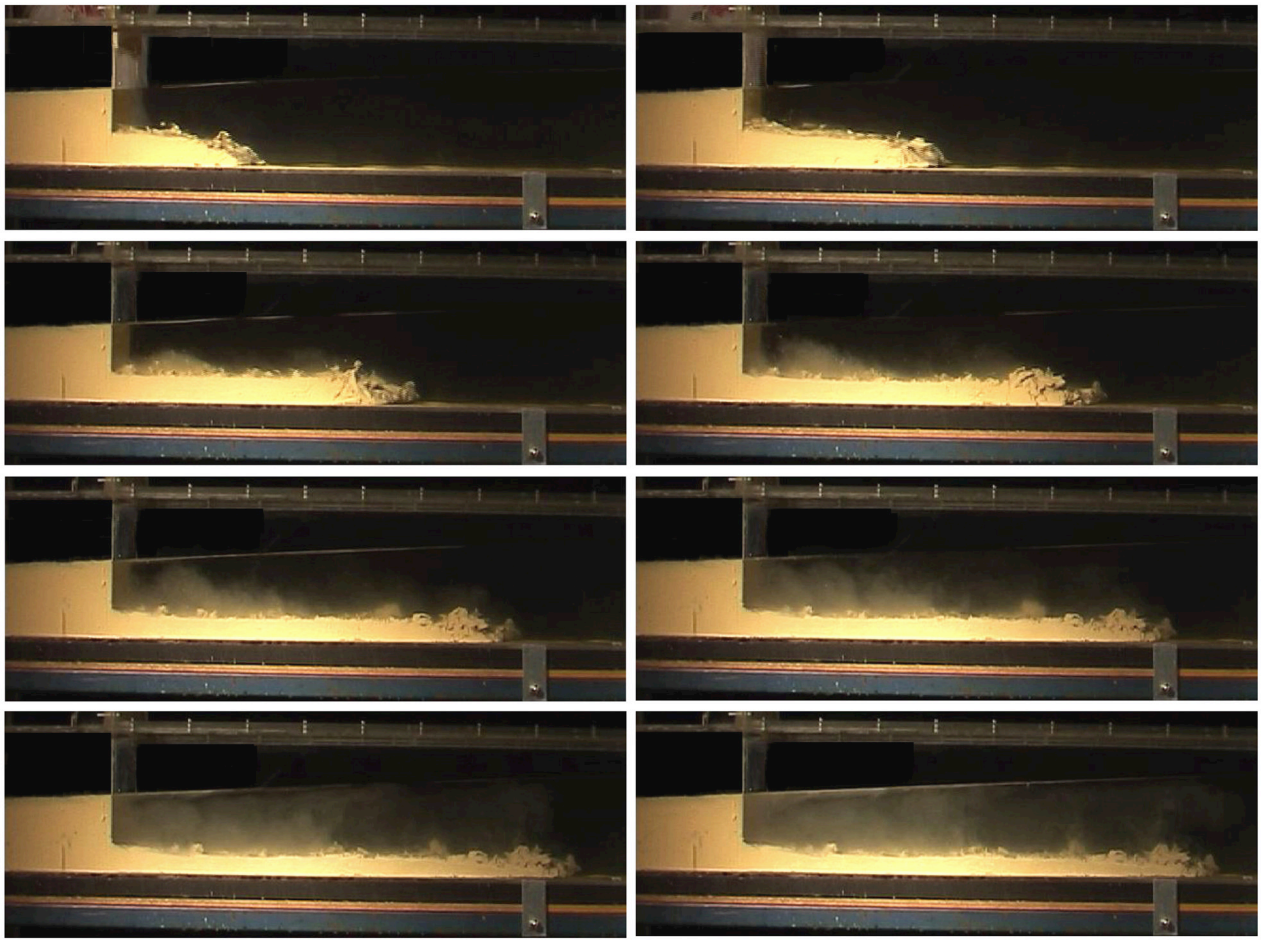

Figure 9. Photographs of the sloping cooling viscoplastic experiment SCP-17. The field of view in each frame is about 1 m. Frames were taken at 1.7, 2.5, 3.8, 5.2, 8.2, 13.0, 28.5, and 44.9 s after the lock was released.

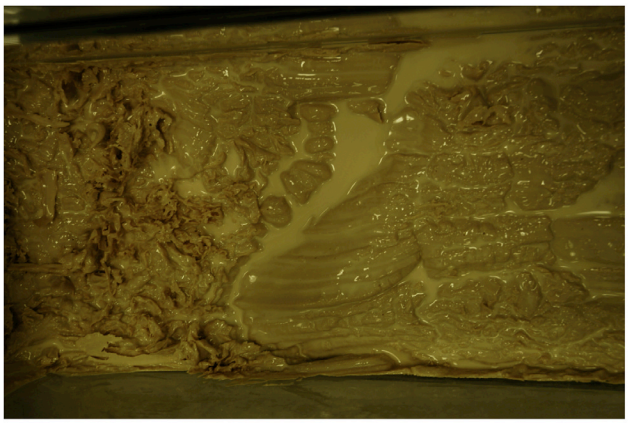

Figure 10. Overhead view of experiment SCP-18, where the flow was from left to right. The image shows a section of the flow where the crust has fractured and rifted, enabling warm underlying slurry to extrude out onto the surface of the flow. The extrusion has a much smoother flow surface, with grooves parallel to the flow direction.

300 Pa found for the same slurry composition (33.3% kaolin) on a horizontal base. This large difference in estimated crust strength probably reflects the very different height profiles of sloping and horizontal flows, which makes it harder for the growing surface crust to stop slope flows rather than horizontal flows. In equation (30), the average flow depth q/L^* is being used to estimate σ_c. In the sloping viscoplastic flows, the thickness is reasonably constant and the flow front thickness is similar to the average depth (Figure 12), so equation (30) should provide a reasonable estimate of σ_c. In contrast, the horizontal viscoplastic flows in Figure 13 decrease substantially in thickness toward the flow front. In this case, the flow front thicknesses are much less than the average flow depths, which results in equation (30) giving large overestimates of σ_c.

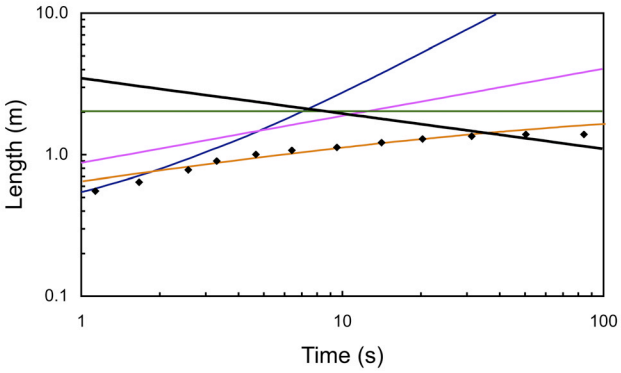

Figure 11. Flow length as a function of time for solidifying slurry experiment SCP-13 on a 3° with Ψ_{sl} = 1.81. The curves show the slumping regime (dark blue line), the sloping viscous flow regime (pink line), the box model of section 2.2 for sloping viscoplastic flow with σ_0 = 3 Pa (orange line), the yield strength limit (green line), and the crust strength regime (black line) given by equation (24), where c_c = 1 and σ_c = 1240 Pa.

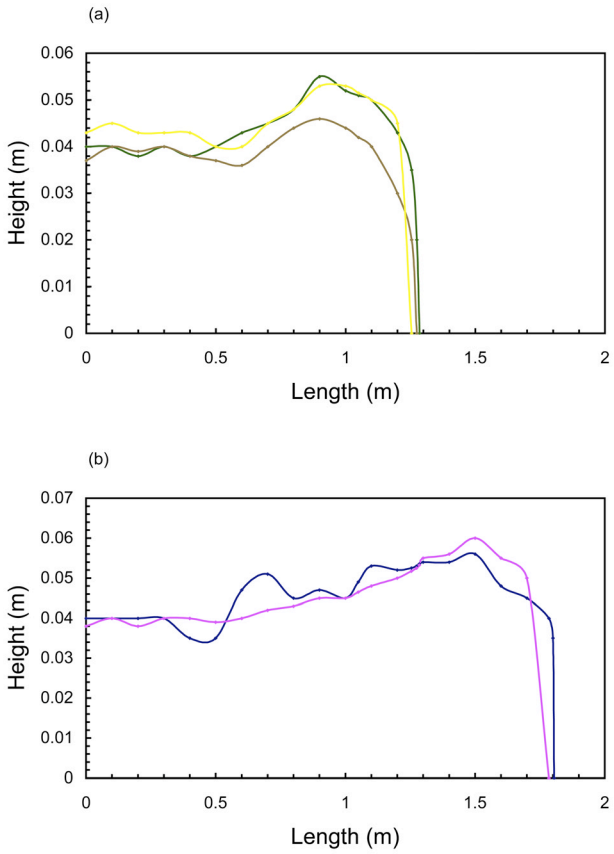

Figure 12. Flow height as a function of length for five solidifying slurry experiments on a slope: (a) SCP-14 (dark blue line), SCP-16 (pink line), and SCP-17 (purple line) and (b) SCP-18 (orange line) and SCP-19 (green line).

8. Application to Lava Flows

[33] In sections 5, 6 and 7, we have shown that the spreading of our experimental fluids on a slope was governed by a number of competing flow regimes, involving inertial flow, viscous flow, viscoplastic flow, and surface solidification at the flow front. In this section, we illustrate how these flow regimes may be used to predict the spreading of lava flows. In our calculations, we assume that a fixed volume of lava is instantaneously released on a gentle slope.

8.1. Solidifying Lava Flows Without a Yield Strength

[34] We first consider the two-dimensional, subaerial breakout on a 3° slope of various quantities of Hawaiian basaltic lava with no internal yield strength. The lava is taken to have a density ρ = 2600 kg m^{-3}, a viscosity η = 100 Pa s and a thermal diffusivity $\kappa = 10^{-6}$ m^{2}s^{-1}. We set the unknown constant c_c equal to 1, and assume a crust yield strength σ_c that lies between 10^4 Pa (as estimated by *Blake and Bruno* [2000, p. 194]) and 10^5 Pa.

[35] Figure 15a shows the predicted spread from a small lava breakout that is on the scale of a pahoehoe lobe or toe

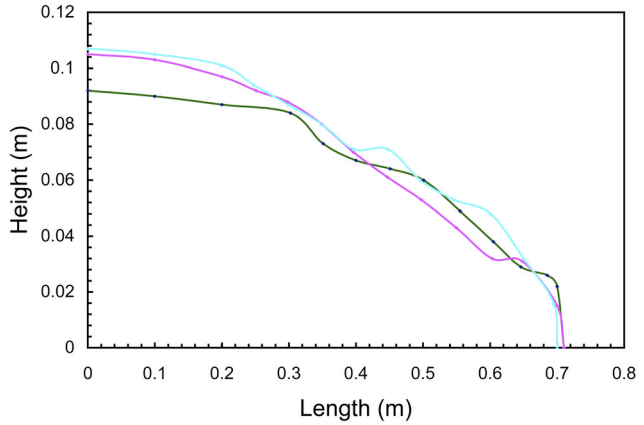

Figure 13. Flow height as a function of length for three solidifying slurry experiments on a horizontal base [*Lyman et al.*, 2005], HCB-27 (pink line), HCB-28 (dark blue line), and HCB-30 (green line).

[*Gregg and Keszthelyi*, 2004], with an initial depth H_0 = 0.3 m and length L_0 = 3 m. This flow is unable to spread in the slumping regime (since the slumping regime curve lies above the viscous flow regime curves in Figure 15a). Instead, it initially spreads in the horizontal viscous flow regime (equation (3)) for a couple of seconds, before undergoing a transition to the sloping viscous flow regime (equation (5)). It then propagates to 7–14 m (after 15–112 s) before the growing surface crust is able to stop the flow.

[36] Figure 15b shows the spread from a medium-sized lava breakout, with an initial depth H_0 = 1 m and length L_0 = 10 m, which could be briefly released from a lava tube or channel. The flow initially spreads in the slumping regime until it undergoes a transition at about 40 m to the sloping viscous flow regime. Depending on the crust yield strength, it then propagates to 57–110 m (after 1–7 min) before the surface crust stops the flow.

[37] In Figure 15c, the spread from a large lava breakout is shown, in which the initial depth H_0 = 3 m and the length L_0 = 30 m. This flow initially spreads in the slumping regime until it undergoes a transition at about 300 m to the sloping viscous flow regime. It then propagates to 400–700 m (in 3–26 min) before the surface crust stops the flow.

[38] When we compare our calculations (compare Table 4) with those made for flow on a horizontal surface [see

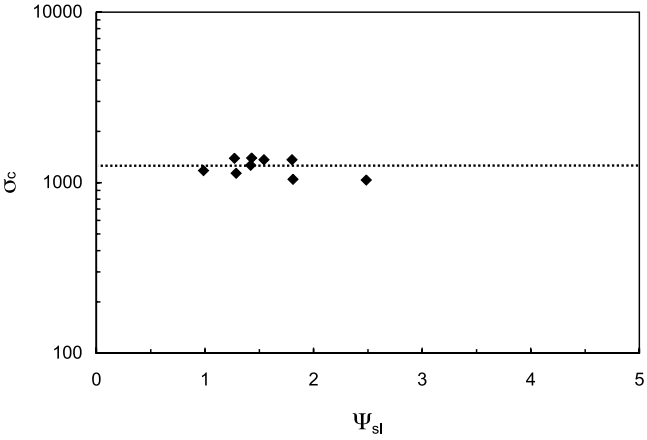

Figure 14. Estimated crust strength σ_c versus Ψ_{sl}, for the solidifying viscoplastic experiments. The strength is constant and has a value of 1240 ± 150 Pa, which is represented by the horizontal dotted line.

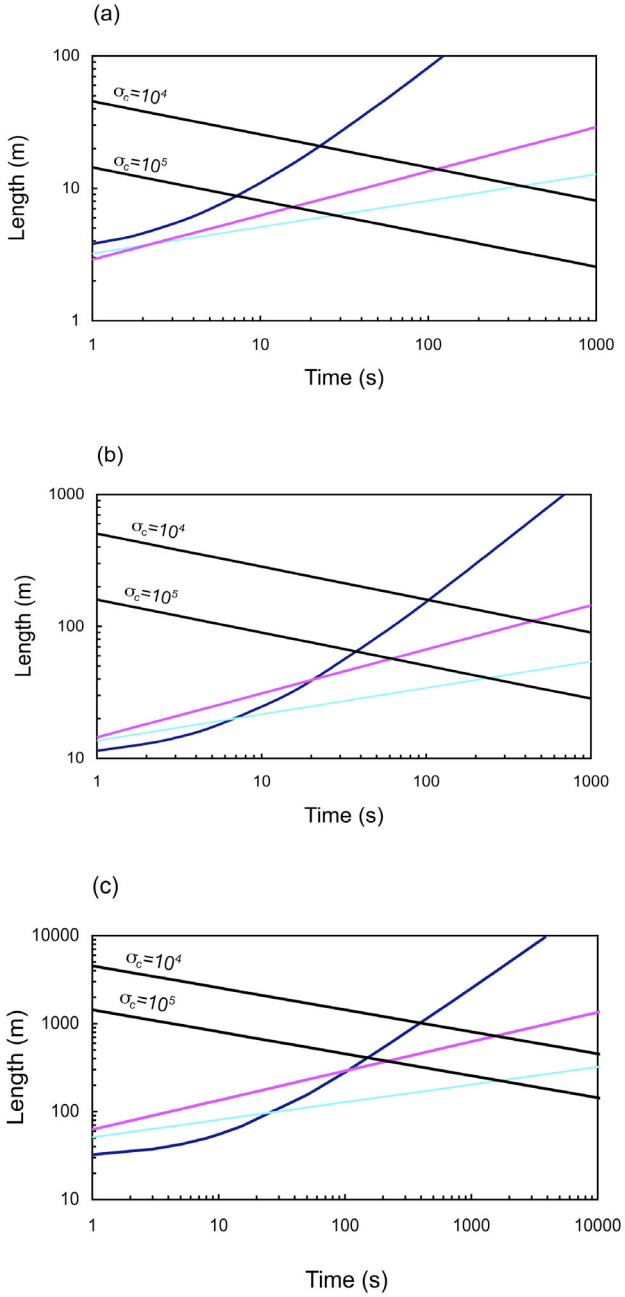

Figure 15. Length as a function of time for various quantities of a Hawaiian lava with a crust yield strength and no yield strength: (a) H_0 = 0.3 m and L_0 = 3 m; (b) H_0 = 1 m and L_0 = 10 m; and (c) H_0 = 3 m and L_0 = 30 m. The curves show the inertial slumping regime (equation (1); dark blue line), the horizontal viscous flow regime (equation (3); light blue line), the sloping viscous flow regime (equation (5); pink line), and the crust strength regime for surface crust yield strengths of 10^4 Pa or 10^5 Pa (equation (22); black lines).

Table 4. Predicted Runout Rime t_c^{vs}, Runout Length L_c^{vs}, and Average Flow Height $H(t_c^{vs})$ for the Flow Down a Slope of Different Quantities of a Hawaiian Lava Without an Internal Yield Strength

			$\sigma_c = 10^4$, Pa			$\sigma_c = 10^5$, Pa		
Size	H_0, m	L_0, m	t_c^{vs}, s	L_c^{vs}, m	$H(t_c^{vs})$, m	t_c^{vs}, s	L_c^{vs}, m	$H(t_c^{vs})$, m
Small	0.3	3	112	14.0	0.064	15.4	7.20	0.125
Medium	1	10	443	110	0.091	61.6	56.9	0.176
Large	3	30	1560	723	0.124	217	375	0.240

Lyman et al., 2005, Table 9], we find that the 3° slope results in increased runout lengths and greatly decreased runout times, particularly at larger flow volumes and smaller crust yield strengths. This result reflects the fact that (25) and (27) imply that $t^{vs}/t_c^v \propto q^{-20/63}\,\sigma_c^{16/63}$, while (26) and (28) imply that $L_c^{vs}/L_c^v \propto q^{5/63}\sigma_c^{-4/63}$.

8.2. Solidifying Lava Flows With a Yield Strength

[39] We next consider the two-dimensional, subaerial breakout on a 10° slope of various quantities of a 1975 Mount Etna basaltic lava composed of about 45% crystals, which had a yield strength of $\sigma_0 = 370 \pm 30$ Pa and a Bingham viscosity of $\eta = 9400 \pm 1500$ Pa s [*Pinkerton and Sparks*, 1978]. We set the unknown constant c_c equal to 1, and assume the lava has a density $\rho = 2600$ kg m^{-3}, a thermal diffusivity $\kappa = 10^{-6}$ m^2 s^{-1} and a crust yield strength σ_c of 10^6 Pa.

[40] Figure 16a shows the spread from a small lava breakout, with an initial depth $H_0 = 2$ m and length $L_0 = 5$ m, which could be briefly released from a lava tube or channel. In contrast to the Hawaiian lava in Figure 15b, this more viscous lava is unable to spread in the slumping regime (since the slumping regime curve lies above the two viscous flow regime curves in Figure 16a). Instead, the lava will spread in the sloping viscoplastic flow regime, until the crust strength stops the flow after 62 s, at a flow length of 18 m and an average flow depth of 0.56 m (see Table 5).

[41] In Figure 16b, we show the spread from a medium-sized breakout of Mount Etna lava, with an initial depth $H_0 = 6$ m and length $L_0 = 15$ m. The flow initially spreads in the slumping regime, for about 40 m. It then undergoes a transition to the sloping viscoplastic flow regime, which it then follows until the crust strength stops the flow at 216 s, at a flow length of 118 m and an average flow depth of 0.76 m (see Table 5).

[42] In Figure 16c, we show the spreading of a large breakout of Mount Etna lava, with a depth $H_0 = 20$ m and a length $L_0 = 50$ m. The flow initially spreads in the slumping regime, for about 400 m. It then undergoes a transition to the sloping viscoplastic flow regime, which it follows until a transition to the crust strength regime after 14 min, at a runout length of 938 m and an average flow depth of 1.07 m (see Table 5).

[43] From these calculations (Table 5), we conclude that a factor of 10 increase in Mount Etna lava volume results in about a factor of 4 increase in runout time and a factor of 7 increase in runout length. When our results are compared with those for flow of a Mount Etna lava on a horizontal surface [see *Lyman et al.*, 2005, Table 10], we find that the 10° slope results in increased runout lengths and greatly decreased runout times, particularly at larger flow volumes. We also observe that all the above lava flows on a slope were stopped by the growing surface

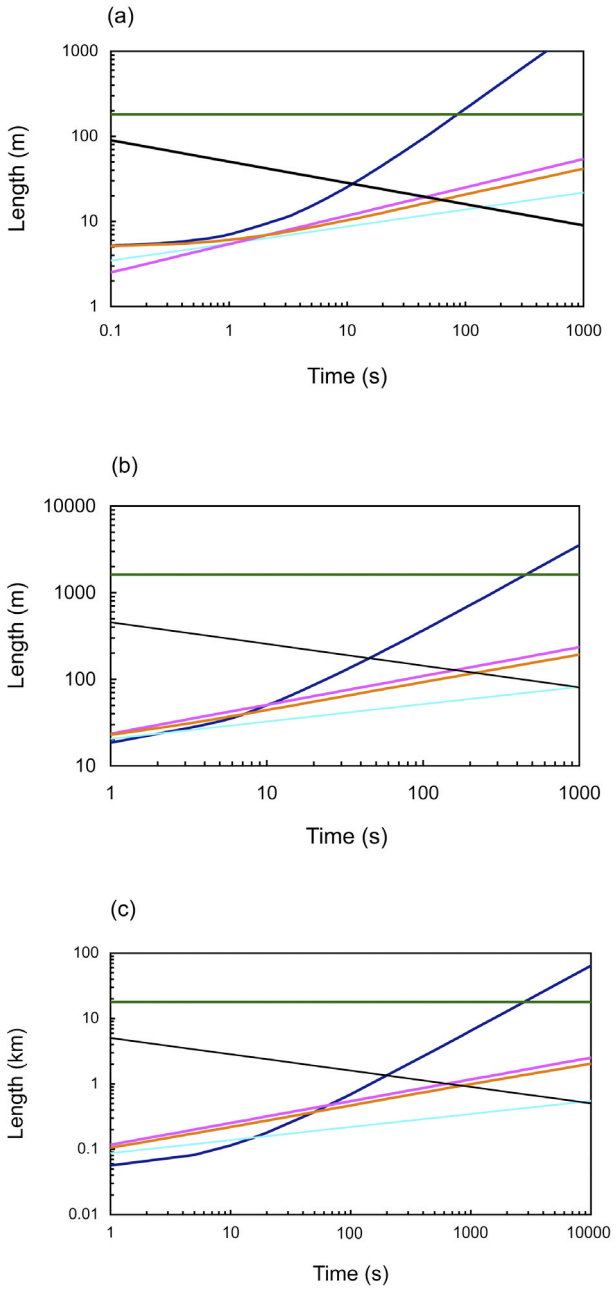

Figure 16. Length as a function of time for various quantities of a Mount Etna lava with a yield strength: (a) $H_0 = 2$ m and $L_0 = 5$ m; (b) $H_0 = 6$ m and $L_0 = 15$ m; and (c) $H_0 = 20$ m and $L_0 = 50$ m. The curves show the inertial slumping regime (equation (1); dark blue line), the horizontal viscous flow regime (equation (3); light blue line), the sloping viscous flow regime (equation (5); pink line), the internal yield strength limit (equation (10); green line), the sloping viscoplastic flow model of section 2.2 (orange line), and the crust strength regime (equation (22); black line).

Table 5. Predicted Runout Time t_c^{vps}, Runout Length L_c^{vps}, and Average Flow Height $H(t_c^{vps})$ for the Flow Down a Slope of Different Quantities of a Mount Etna Lava With an Internal Yield Strength

Size	H_0, m	L_0, m	t_c^{vps}, s	L_c^{vps}, m	$H(t_c^{vps})$, m	L_y, m
Small	2	5	62.4	18.0	0.56	180
Medium	6	15	216	119	0.76	1622
Large	20	50	839	938	1.07	18030

crust, rather than the internal yield strength (Figure 16). This result contrasts with calculations for similar lava flows on a horizontal surface [*Lyman et al.*, 2005], where small flows were stopped by the surface crust while larger flows were stopped by the internal yield strength. Finally, we note that there is little difference between the curves denoting the sloping viscoplastic regime and the sloping viscous regime in Figure 16, because the flow depths H are always much greater than H_y = 0.084 m. The internal yield strength therefore has little effect on these lava flows.

9. Conclusions

[44] In this paper we have examined the two-dimensional flow of a fixed volume of lava rapidly released on horizontal and sloping surfaces. A number of the dynamical flow laws are presented, which are verified by laboratory experiments and then extrapolated to predict the downslope flow of lava breakouts at Hawaii and Mount Etna. We have found that five different flow regimes can arise:

[45] 1. A slumping regime, where the lava initially moves at a constant velocity. This regime will arise for moderate to large breakouts of Hawaiian and Mount Etna lava (Figures 15 and 16).

[46] 2. A horizontal viscous regime, which arises immediately for very small breakouts of Hawaiian lava (Figure 15a).

[47] 3. A sloping viscous regime, which follows either the slumping regime or the horizontal viscous regime during the flow of a Hawaiian lava that has no internal yield strength (Figure 15).

[48] 4. A sloping viscoplastic regime, which either arises immediately or follows the slumping regime during the flow of a Mount Etna lava with an internal yield strength (Figure 16).

[49] 5. A surface crust strength regime where the yield strength σ_c of the growing surface crust eventually stops the downslope lava flow. This regime stops all breakouts of the Hawaiian and Mount Etna lavas, regardless of the quantity of lava released (Figures 15 and 16).

Notation

c_c constant in surface crust flow law.
c_{sl} constant in slumping flow law.
c_v constant in horizontal viscous flow law.
c_{vs} constant in sloping viscous flow law.
g acceleration due to gravity.
H average flow depth.
H_0 average initial height of the fluid in the reservoir.
H_y final static height of an isothermal yield strength flow on a slope.
H^* final flow depth.
L flow length.
L_0 initial length of the reservoir.
L_{vs}^v transition length from the horizontal viscous regime to the viscous slope regime.
L_c^v transition length from the horizontal viscous regime to crust strength regime.
L_c^{vs} transition length from the viscous slope regime to crust strength regime.
L_c^{vps} transition length from the viscoplastic slope regime to crust strength regime.
L_y theoretical limit of an isothermal yield strength flow on a slope.
L^* final flow length.
Pe Péclet number.
q fluid volume per unit channel width.
Re Reynolds number.
t time.
t_s solidification timescale.
t_{vs}^v transition time from the horizontal viscous regime to the sloping viscous regime.
t_c^v transition time from the horizontal viscous regime to crust strength regime.
t_c^{vs} transition time from the viscous slope regime to crust strength regime.
t_c^{vps} transition time from the viscoplastic slope regime to crust strength regime.
t^* time required to reach the final flow length.
U surface flow velocity.
U_p plug velocity of a viscoplastic flow on a slope.
β channel slope (measured from horizontal).
δ surface crust thickness.
$\Delta\rho$ density difference between the flow and the ambient fluid.
η viscosity of the flows (lava, PEG, slurry).
κ thermal diffusivity of the flows (lava, PEG, slurry).
Ψ_{sl} dimensionless parameter in the slumping flow regime, defined by the ratio of the solidification timescale to the advection timescale [*Lyman et al.*, 2005].
ρ density of the flow (lava, PEG, or slurry).
ρ_a density of the ambient fluid.
σ_0 internal yield strength of the lava.
σ_c yield strength of the surface crust.
τ timescale of a viscoplastic flow on a slope.
ξ dimensionless depth of viscous flow in a viscoplastic flow.
ξ_0 initial dimensionless depth of viscous flow in a viscoplastic flow.

[50] **Acknowledgments.** We wish to thank Ross Griffiths for advice and helpful comments and Tony Beasley and Chris Morgan for technical assistance in the laboratory. We gratefully acknowledge financial support from the Australian Research Council (ARC grant DP0342569).

References

Balmforth, N. J., and R. V. Craster (2000), Dynamics of cooling domes of viscoplastic fluid, *J. Fluid Mech.*, *422*, 225–248.

Balmforth, N. J., A. S. Burbidge, R. V. Craster, J. Salzig, and A. Shen (2000), Visco-plastic models of isothermal lava domes, *J. Fluid Mech.*, *403*, 37–65.

Balmforth, N. J., R. V. Craster, and R. Sassi (2002), Shallow viscoplastic flow on an inclined plane, *J. Fluid Mech.*, *470*, 1–29.

Balmforth, N. J., R. V. Craster, and R. Sassi (2004), Dynamics of cooling viscoplastic domes, *J. Fluid Mech.*, *499*, 149–182.
Blake, S. (1990), Viscoplastic models of lava domes, in *Lava Flows and Domes: Emplacement Mechanisms and Hazard Implications*, edited by J. H. Fink, pp. 88–126, Springer, New York.
Blake, S., and B. C. Bruno (2000), Modelling the emplacement of compound lava flows, *Earth Planet. Sci. Lett.*, *184*, 181–197.
Cashman, K. V., R. C. Kerr, and R. W. Griffiths (2006), A laboratory model of surface crust formation and disruption on channelized lava fows, *Bull. Volcanol.*, online first, doi:10.1007/s00445-005-0048.z.
Fink, J. H., and R. W. Griffiths (1990), Radial spreading of viscous-gravity currents with solidifying crust, *J. Fluid Mech.*, *221*, 485–509.
Gregg, T. K. P., and J. H. Fink (2000), A laboratory investigation into the the effects of slope on lava flow morphology, *J. Volcanol. Geotherm. Res.*, *96*, 145–159.
Gregg, T. K. P., and L. P. Keszthelyi (2004), The emplacement of pahoehoe toes: Field observations and comparison to laboratory simulations, *Bull. Volcanol.*, *66*, 381–391.
Griffiths, R. W. (2000), The dynamics of lava flows, *Annu. Revs. Fluid Mech.*, *32*, 477–518.
Griffiths, R. W., and J. H. Fink (1993), Effects of surface cooling on the spreading of lava flows and domes, *J. Fluid Mech.*, *252*, 667–702.
Griffiths, R. W., and J. H. Fink (1997), Solidifying Bingham extrusions: A model for the growth of silicic lava domes, *J. Fluid Mech.*, *347*, 13–36.
Griffiths, R. W., R. C. Kerr, and K. V. Cashman (2003), Patterns of solidification in channel flows with surface cooling, *J. Fluid Mech.*, *496*, 33–62.
Hallworth, M. A., H. E. Huppert, and R. S. J. Sparks (1987), A laboratory simulation of basaltic lava flows, *Mod. Geol.*, *11*, 93–107.
Huang, X., and M. H. Garcia (1998), A Herschel-Bulkley model for mud flow down a slope, *J. Fluid Mech.*, *374*, 305–333.
Hulme, G. (1974), The interpretation of lava flow morphology, *Geophys. J. R. Astron. Soc.*, *39*, 361–383.
Huppert, H. E. (1982a), Flow and instability of a viscous current down a slope, *Nature*, *30*, 427–429.
Huppert, H. E. (1982b), The propagation of two-dimensional and axisymmetric viscous gravity currents over a rigid horizontal surface, *J. Fluid Mech.*, *121*, 43–58.
Huppert, H. E. (1998), Quantitative modelling of granular suspension flows, *Philos. Trans. R. Soc. London, Ser. A*, *356*, 2471–2496.
Johnson, A. M. (1970), *Physical Processes in Geology*, W. H. Freeman, New York.
Lister, J. R. (1992), Viscous flows down an inclined plane from point and line sources, *J. Fluid Mech.*, *242*, 631–653.
Lister, J. R., and R. C. Kerr (1994), Influence of cooling on lava-flow dynamics—Comment, *Geology*, *22*, 93–94.
Lui, K. F., and C. C. Mei (1989), Slow spreading of a sheet of Bingham fluid on an inclined plane, *J. Fluid Mech.*, *207*, 505–529.
Lyman, A. W., E. Koenig, and J. H. Fink (2004), Predicting yield strengths and effusion rates of lava domes from morphology and underlying topography, *J. Volcanol. Geotherm. Res.*, *129*, 125–138.
Lyman, A. W., R. W. Kerr, and R. W. Griffiths (2005), The effects of internal rheology and surface cooling on the emplacement of lava flows, *J. Geophys. Res.*, *110*, B08207, doi:10.1029/2005JB003643.
Mei, C. C., and M. Yuhi (2001), Slow flow of a Bingham fluid in a shallow channel of finite width, *J. Fluid Mech.*, *431*, 135–159.
Nye, J. F. (1965), The flow of a glacier in a channel of rectangular, elliptic or parabolic cross-section, *J. Glaciol.*, *5*, 661–690.
Osmond, D. I., and R. W. Griffiths (2001), The static shape of yield strength fluids slowly emplaced on slopes, *J. Geophys. Res.*, *106*, 16,241–16,250.
Pattle, R. E. (1959), Diffusion from an instantaneous point source with a concentration-dependent coefficient, *Q. J. Mech. Appl. Math.*, *12*, 407–409.
Pinkerton, H., and R. S. J. Sparks (1978), Field measurements of the rheology of lava, *Nature*, *276*, 383–385.
Rottman, J. W., and J. E. Simpson (1983), Gravity currents produced by instananeous releases of a heavy fluid in a rectangular channel, *J. Fluid Mech.*, *135*, 95–110.
Simpson, J. E. (1997), *Gravity Currents in the Environment and the Laboratory*, 2nd ed., Cambridge Univ. Press, New York.
Stasiuk, M. V., C. Jaupart, and R. S. J. Sparks (1993), Influence of cooling on lava-flow dynamics, *Geology*, *21*, 335–338.
Tallarico, A., and M. Dragoni (1999), Viscous newtonian laminar flow in a rectangular channel: Application to etna lava flows, *Bull. Volcanol.*, *61*, 40–47.
Tallarico, A., and M. Dragoni (2000), A three-dimensional bingham model for channeled lava flows, *J. Geophys. Res.*, *105*, 25,969–25,980.

R. C. Kerr and A. W. Lyman, Research School of Earth Sciences, Australian National University, Jaeger 7, Canberra, ACT 0200, Australia. (aaron.lyman@anu.edu.au)